3
Determination of Band Alignment at 2D/3D Heterointerfaces

3.1 INTRODUCTION

The most widely studied TMDs such as MoS_2, WS_2, $MoSe_2$, and WSe_2 have sparked a renewed research interest in nanoelectronics and optoelectronics due to due to their tunable bandgap, large carrier mobility, optical transparency, and mechanical flexibility(Splendiani et al., 2010). In recent years, MoS_2, the frontrunner of TMDs family, has grabbed a great research interest in designing electronic and optoelectronic devices due to its unique electrical, mechanical, and optical properties. The weak van der Waals force present among different layers of MoS_2 facilitates the isolation of monolayer to few-layer from the bulk crystal. Monolayer MoS_2 based transistor possesses very high mobility of 200 cm^2/ V.s, with a current on/off ratio of 10^8. These improved traits were obtained by introducing high-k dielectric, which results in suppression of Coulomb scattering and modification of phonon dispersion(Radisavljevic et al., 2011).

Recently, MoS_2 based vdW heterostructures have opened up new avenues due to their appealing electronic and optoelectronic applications(Li et al., 2016). These vdW heterostructures have been developed by stacking different 2D materials. These vdW heterojunctions are very conducive for photodetectors, light-emitters, and field-effect transistors(Wang et al., 2014). The exciting new physics at the interface plays a major role in optimizing the performance of the heterojunction based devices. For example, Hua et al. have controlled the catalytic performance of MoS_2/graphene oxide heterojunction by oxygen species interface hybridization(Hua et al., 2018).

The exact measurement of the valence band offset (VBO) and conduction band offset (CBO) values are of prime importance in exploring new opportunities and addressing formidable challenges for designing futuristic high-performance devices. The valance and conduction band offsets are having several noticeable implications, including the modulation of the resistance at the interfacese(Majee et al., 2017). The CBO and VBO values have already been determined for a number of different kinds of heterojunctions in the earlier reports, such as GaN/WSe_2, and MoS_2/WSe_2 (Chiu et al., 2015; Goel et al., 2018; Tangi et al., 2017). The determination of discontinuities at the interface paves the way for the integration of atomically thin 2D semiconductors with other materials for investigating their unprecedented functionalities.

A large number of MX_2 based heterostructures have already been used for optoelectronic applications because of their strong light-matter interactions. Most of the MX_2 based heterostructures possess type II band alignment resulting in promising photovoltaic and optoelectronic applications due to efficient separation of photoinduced charge carriers. Hong et al. have demonstrated an ultrafast charge transfer at MoS_2/WS_2 heterointerface(Hong et al., 2014). Figure 3.1(a) shows the band diagram of MoS_2 and WS_2 before making contact, while Figure 3.1(b) illustrates the Fermi level shifting after forming the contact. An efficient charge transfer at type II heterointerface is shown in Figure 3.1(c). From the generated electron-hole pairs in MoS_2 upon optical irradiation, electron remains in MoS_2 while hole got transferred to WS_2. A hole transfers from MoS_2 to WS_2 took less than 50 fs under optical irradiation. The

ultrafast response is due to the atomically thin nature of MoS_2 and WS_2. During the charge transfer process, the photoexcited charge carriers have to travel only a few nm distances due to atomic thin nature of constituent semiconductors.

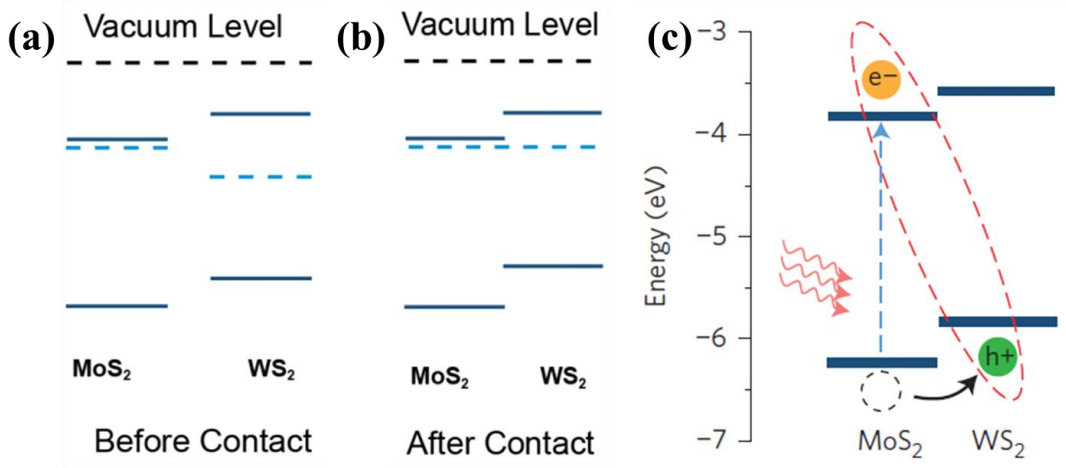

Figure 3.1: Band-diagram of MoS_2 and WS_2 (a) before making contact and (b) after making contact. Once the contact took place, the Fermi level becomes constant. (c) Type-II band alignment at MoS_2/WS_2 heterointerface depicting efficient hole transfer from MoS_2 to WS_2. (Source: Hong et al., 2014)

Furthermore, the barrier height and performance of heterojunction is also strongly dependent on the band alignment at the interface(Kraut et al., 1980). To study the band alignment at MoS_2- silicon and MoS_2-GaN heterojunctions, we have measured the VBO and CBO values at the heterointerfaces using X-ray photoelectron spectroscopy (XPS) and Ultraviolet photoelectron spectroscopy (UPS). Depending on the type of band alignment, the hybrid heterojunctions can be utilized for various potential applications, including optoelectronic devices(Wang et al., 2014), quantum well structures(Tangi et al., 2017), and tunnel diodes(Krishnamoorthy et al., 2016). Thus, the determination of band offset values and type of band alignment at heterojunctions is essential to pave the way for the integration of transition metal dichalcogenides with other materials.

In addition, most of the previous research has focused on monolayer MoS_2 and the hidden potential of few layer MoS_2 (FL-MoS_2) remains unexplored. Monolayer MoS_2 showed a contact resistance and mobility of 740 KΩ.µm and 13 $cm^2/V.s$ respectively, while 5 layer MoS_2 unveils a considerable lower contact resistance and higher mobility of 1.56 KΩ.µm and 52 $cm^2/V.s$ respectively, with Ti(10 nm)/Au(100 nm) contacts(Liu et al., 2013). Kwon et al.(Kwon et al., 2017) have also reported a Schottky barrier height as low as 70 meV and a higher mobility of 23.9 $cm^2/V.s$ for trilayer thick MoS_2 with Al contacts. Therefore, here we choose FL-MoS_2 because of its lower contact resistance with Au which results in increasing the on-current and the mobility of the device.

3.2 BAND OFFSETS AT FEW-LAYER MoS_2/Si HETEROJUNCTION

3.2.1 Fabrication and characterization of MoS_2/Si heterojunction

The device fabrication began with the deposition of Si_3N_4 with a 250-nm thickness on Si substrate using RF sputtering technique with a constant flow of Ar (45 sccm) and N_2 (10 sccm) gas for 1 h. For making the top and back contacts, 200/5-nm thick Au/Cr and 200-nm thick Al were deposited using thermal evaporation under high vacuum conditions. Au made an ohmic contact with MoS_2 while Al made an ohmic contact with Silicon. The MoS_2/Si heterojunction was fabricated by exfoliating FL-MoS_2 from molybdenite crystal (from SPI supply) by using scotch tape and staking it over the structure. Renishaw Raman spectrometer with a laser

excitation wavelength of 514 nm and Park Systems atomic force microscope was used to determine the thickness of the deposited MoS_2 flake.

Figure 3.2 (a and b) shows an optical micrograph of FL-MoS_2 deposited on the p-Si substrate with Au electrode. Raman spectroscopy and AFM measurement have been widely used for studying 2D materials, and mainly for identifying the number of layers. The Raman spectra having peaks of two distinguished vibrational modes E^1_{2g} (in-plane) and A_{1g} (out-of-plane) is located near ~ 384 and ~ 408 cm^{-1}, as shown in Figure 3.2(b). The difference between in-plane and out-of-plane vibrational modes is ~ 24 cm^{-1}, which assures few-layer behavior of exfoliated MoS_2 flake. Our Raman results are consistent with the earlier reports for FL-MoS_2 structure(Lee et al., 2012). The absolute thickness of exfoliated MoS_2 flake is further confirmed by using AFM characterization. Figure 3.3(a) shows the AFM image of FL-MoS_2 and Figure 3.3(b) shows the height profile confirming ~ 3.5 nm of thickness of FL-MoS_2, which is in good agreement with the thickness obtained by Raman spectroscopy. The XPS survey scan of only silicon, only MoS_2, and MoS_2/Si heterojunction is shown in Figure 3.4.

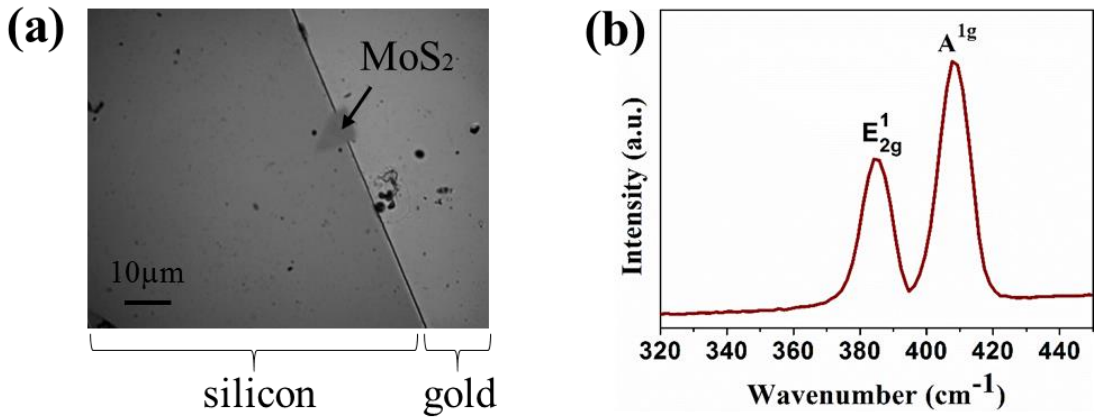

Figure 3.2: Optical microscopy image taken on the stacked MoS_2/Si heterojunction. (c) Raman spectra of the exfoliated FL-MoS_2 obtained using 514nm laser excitation.

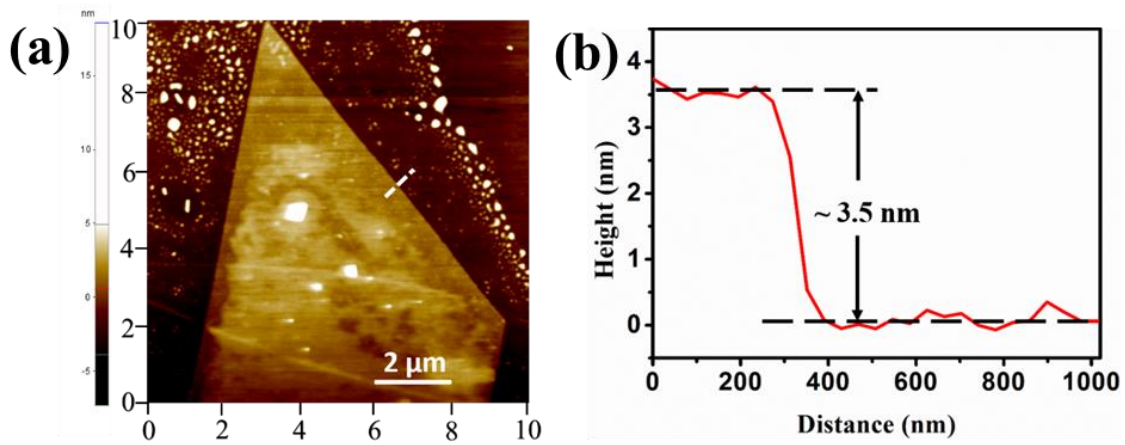

Figure 3.3: AFM characterization. (a) AFM image of the exfoliated FL-MoS_2 on Si and (b) the corresponding height profile along the dotted line.

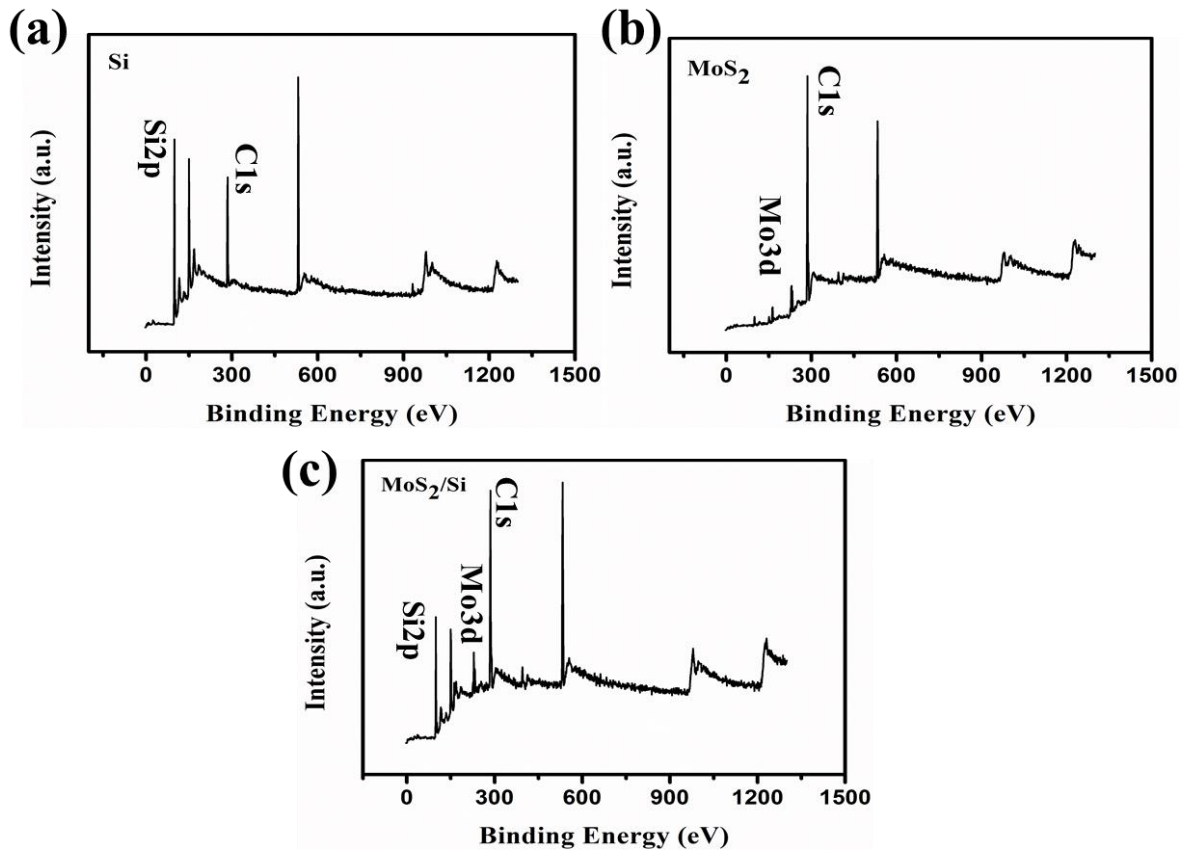

Figure 3.4: XPS survey scan of (a) Si, (b) MoS_2, and (c) MoS_2/Si.

3.2.2 Calculation of VBO through XPS measurement

The method provided by Kraut et al.(Kraut et al., 1980) allows us to calculate the precise value of VBO for MoS_2/Si heterojunction as follows:

$$\Delta E_v = \left(E^{MoS_2}_{Mo3d_{5/2}} - E^{Si}_{Si2p_{3/2}}\right) + \left(E^{Si}_{Si2p_{3/2}} - E^{Si}_{VBM}\right) - \left(E^{MoS_2}_{Mo3d_{5/2}} - E^{MoS_2}_{VBM}\right) \qquad (3.1)$$

where the first term $\left(E^{MoS_2}_{Mo3d_{5/2}} - E^{Si}_{Si2p_{3/2}}\right)$ is the separation in binding energy for Mo 3d and Si 2p core levels of MoS_2/p-Si interface. And the second and third terms are the binding energy difference between the core level and valence band maximum (VBM) of p-Si and MoS_2, respectively. To evaluate VBO at MoS_2/p-Si interface, we need to calculate the energy of core levels relative to VBM of MoS_2 and p-Si individually. The VBM positions are calculated by extrapolating the leading edge of VB spectra(Bhat et al., 2011). VBM values of 0.91 eV for FL-MoS_2 and 0.2 eV for p-Si were deduced from VB spectra of MoS_2 and p-Si, respectively, as shown in Figure 3.5 (a and b). The difference between $Mo3d_{5/2}$ and $Si2p$ core-levels is measured to be 130.17 $\pm$ 0.10 eV at the interface (Figure 3.5 (c)). Now, the value of $Si2p$ relative to the VBM of Si and the value of $Mo3d_{5/2}$ relative to the VBM of MoS_2 are estimated to be 99.03 $\pm$ 0.10 eV and 228.54 $\pm$ 0.10 eV respectively. Thus the value of VBO is estimated to be 0.66 $\pm$ 0.17 eV by using Eq. (3.1).

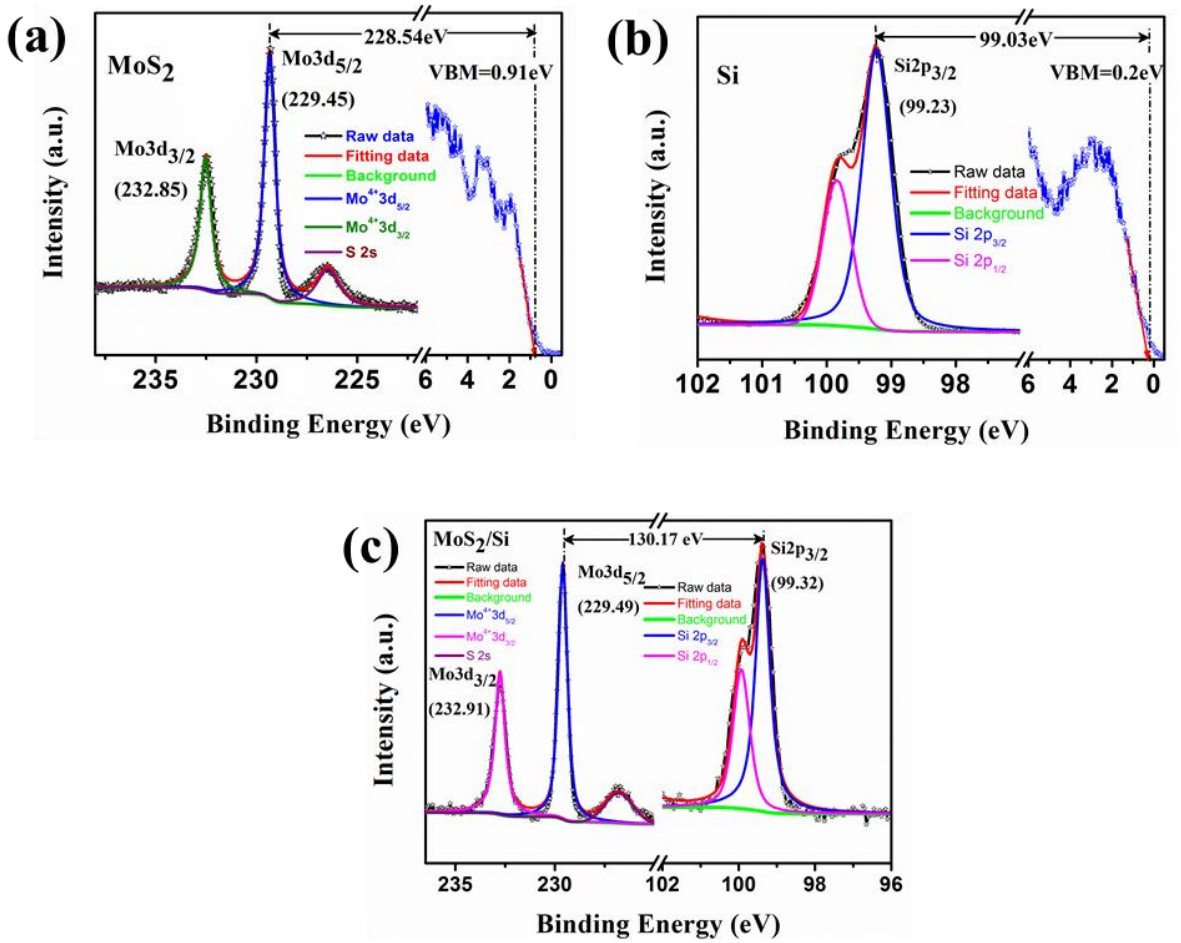

Figure 3.5: The x-ray photoelectron spectroscopy (XPS) spectra for (a) isolated MoS_2 flake, also providing the binding energy separation between Mo 3d core-level and valence band spectra (b) Si substrate, also representing the binding energy separation between Si 2p core-level and valence band spectra and (c) stacked MoS_2/Si heterojunction, showing the binding energy separation between Mo 3d and Si 2p core-levels.

The value of CBO at MoS_2/ p-Si interface can be calculated as follows.

$$\Delta E_c = \Delta E_v + E_g^{Si} - E_g^{MoS_2} \tag{3.2}$$

by substituting the values of VBO ($\Delta E_v = 0.66 \pm 0.17\ eV$), bandgap of Si ($E_g^{Si} = 1.11\ eV$), and MoS_2 ($E_g^{MoS_2} = 1.3\ eV$)(Jiang et al., 2015) in Eq. (3.2), the CBO is measured to be 0.47 $\pm$ 0.17eV.

3.2.3 Calculation of CBO through UPS measurement

We have also confirmed the calculated value of CBO using Anderson's affinity rule(Anderson, 1960), by measuring the difference between electron affinities of FL-MoS_2 and Si. In order to calculate electron affinity, UPS measurement of the constituent materials was performed, as shown in Figure 3.6 (a and b). Electron affinities were determined by using the following relation(Tangi et al., 2017).

$$\chi = h\nu_{He-I} - W - E_g \tag{3.3}$$

where $h\nu_{He-I}$ is the He-I resonance line photon energy (21.22 eV) emitted from neutral atoms, W is the width of emitted electrons, and E_g is the bandgap of constituent materials. The width of emitted electrons is calculated by taking into account the difference between the onset of the secondary electrons and VBM, as shown in Figure 3.6 (a and b).

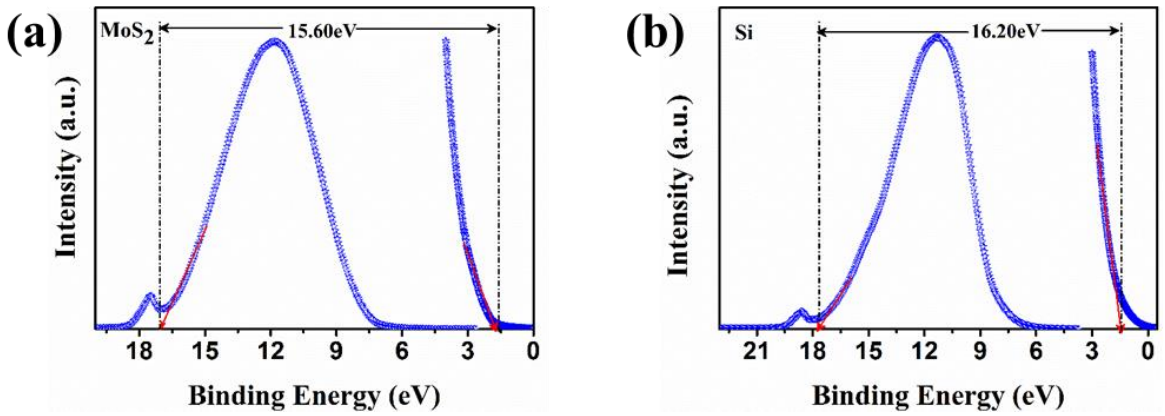

Figure 3.6: (a) and (b) Ultraviolet photoelectron spectroscopy (UPS) spectra for deposited MoS_2 flake and Si substrate.

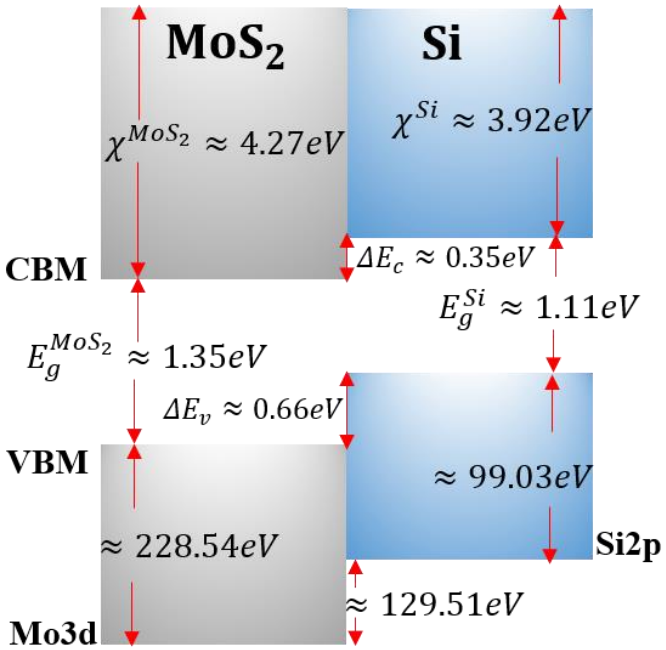

Figure 3.7: Type-II band alignment schematic representation at MoS_2/Si heterojunction.

By using Eq. (3.3) the values of electron affinities were calculated to be 4.32 $\pm$ 0.10 and 3.92 $\pm$ 0.10 eV for MoS_2 and Si, respectively. Thus, in accordance with Anderson's affinity rule, CBO is determined to be 0.40 $\pm$ 0.10 eV. Our obtained CBO value by using UPS is consistent with that of obtained by using XPS (Eq. (3.1)) within the experimental error bar. Hence, the measured VBO and CBO parameters affirm a type-II band alignment at the MoS_2/p-Si interface, as illustrated by the schematic diagram of Figure 3.7.

3.3 BAND OFFSETS AT FEW-LAYER MoS_2/GaN HETEROJUNCTION

The movement of charge carriers across the heterojunction relies mainly on the discontinuities at the interfaces. As a matter of fact, the heterojunctions between the layered transition metal dichalcogenides (TMDs) and wide bandgap group-III nitrides have drawn much interest due to their primary importance in electronic and photonic devices. Our endeavors also include exploring the ultraviolet photodetection capability and gas sensing performance of MoS_2/GaN heterojunction for high-performance electronic devices(Goel et al., 2019; Goel et al., 2018). Ruzmetov et al. have demonstrated a high-performance electronic device based on MoS_2/GaN vertical heterojunction with the desired properties(Ruzmetov et al., 2016). The high quality, unstrained heterostructure showed a 20-fold enhancement in

photoluminescence. A pressure-modulated heterojunction composed of MoS_2 and GaN has also been actualized by Xue. et al. via piezo-phototronic effect(Xue et al., 2017).

3.3.1 Fabrication of MoS_2/GaN heterojunction

3.3.1.1 The growth of GaN film

A ~ 300 nm GaN film was grown on a c-sapphire substrate by using molecular beam epitaxy (MBE) system. Before the growth of GaN film, the sapphire substrate was cleaned thermally at 750 °C for 30 min inside the MBE chamber, followed by the nitridation process for 30 min at 700 °C. The nitridation process was carried out by exposing sapphire substrate into the nitrogen plasma. After the nitridation process, the GaN film was grown on a sapphire substrate using a two-step procedure; low-temperature growth of GaN buffer layer of thickness 20 nm at 500 °C followed by the high-temperature growth of GaN epilayer of thickness 280 nm at 750 °C. During the growth of GaN layers, the RF plasma power and nitrogen flow rate were kept at 350 W and 1 sccm, respectively.

3.3.1.2 Fabrication of MoS_2/GaN heterojunction

The growth of few atomic layers MoS_2 film on the GaN substrate was carried out by a two-step process. Firstly, a thin film of Mo was deposited on the GaN substrate via magnetron sputtering technique by using a Mo target (99.99 % purity). During the growth of Mo film, the DC power, substrate temperature, and Ar gas flow were kept at 40 W, 600 °C, and 40 sccm, respectively. And secondly, the Mo deposited sample was placed in an alumina boat inside the central zone of a 2-inch diameter tube furnace. Another alumina boat containing 1 gm of sulfur was placed at a distance of 12 cm away from the central zone in the horizontal tube furnace. The temperature of the central zone of the furnace was raised from room temperature to 600 °C in 20 min, while the temperature of the other zone containing sulfur was maintained at 220 °C. The furnace was cooled down after 10 min of reaction. The detailed gwowth process of MoS_2 has also explained in the subsequent chapters.

3.3.1.3 Characterization

The PL spectra of MBE grown GaN film at room temperature is shown in Figure 3.8. A strong emission peak ~ 365 nm wavelength was observed. Few-layer MoS_2 does not show a strong PL spectrum due to its indirect bandgap; therefore, we have shown PL spectra of only GaN film. The surface morphology of the as-fabricated MoS_2 was examined by field emission scanning electron microscopy (Tecnai G^2 20 (FEI) S-Twin). The growth of MoS_2 film on GaN substrate is shown in Figure 3.9. The structural quality and crystallinity of the MoS_2/GaN heterojunction were characterized by Raman spectroscopy (Renishaw single monochromator with a 514 nm laser excitation) and XRD (Panalytical X Pert Pro) measurements. The XPS and UPS measurements were carried out by Scienta Omicron multiprobe spectroscopy system using monochromatic Al-Kα x-ray radiative source (1486.7 eV) and He I ($h\nu$=21.22 eV) photon source, respectively.

As shown in Figure 3.10(a), Raman spectra depict two typical vibrational modes at 383 and 407 cm^{-1}, which correspond to in-plane (E^1_{2g}) and out-of-plane (A_{1g}) active modes of MoS_2. The spacing of ~ 24 cm^{-1} between E^1_{2g} and A_{1g} scattering modes corresponds to a few-layer MoS_2(Lee et al., 2010; Tsai et al., 2013). The two other Raman peaks observed at 568 and 734 cm^{-1} belong to E_2 and A_1 longitudinal modes of the GaN film(Limmer et al., 1998). Figure 3.10(b) illustrates the structural details of the MoS_2/GaN heterojunction using XRD patterns. The as-grown MoS_2 film reveals distinct diffracted peaks at 14.3°, 25.6°, 39.1°, and 58.4° corresponding to (002), (004), (103), and (110) crystals planes(Dwivedi et al., 2017; Yan et al., 2015). In addition, the other peak observed at 34.5° was attributed to (002) crystal plane of GaN films (JCPDS Card No. 37-1492), indicating c-plane orientation growth of the epitaxial film(Roul et al., 2011). The XPS survey scan of only GaN, only MoS_2, and MoS_2/GaN heterojunction is shown in Figure 3.11.

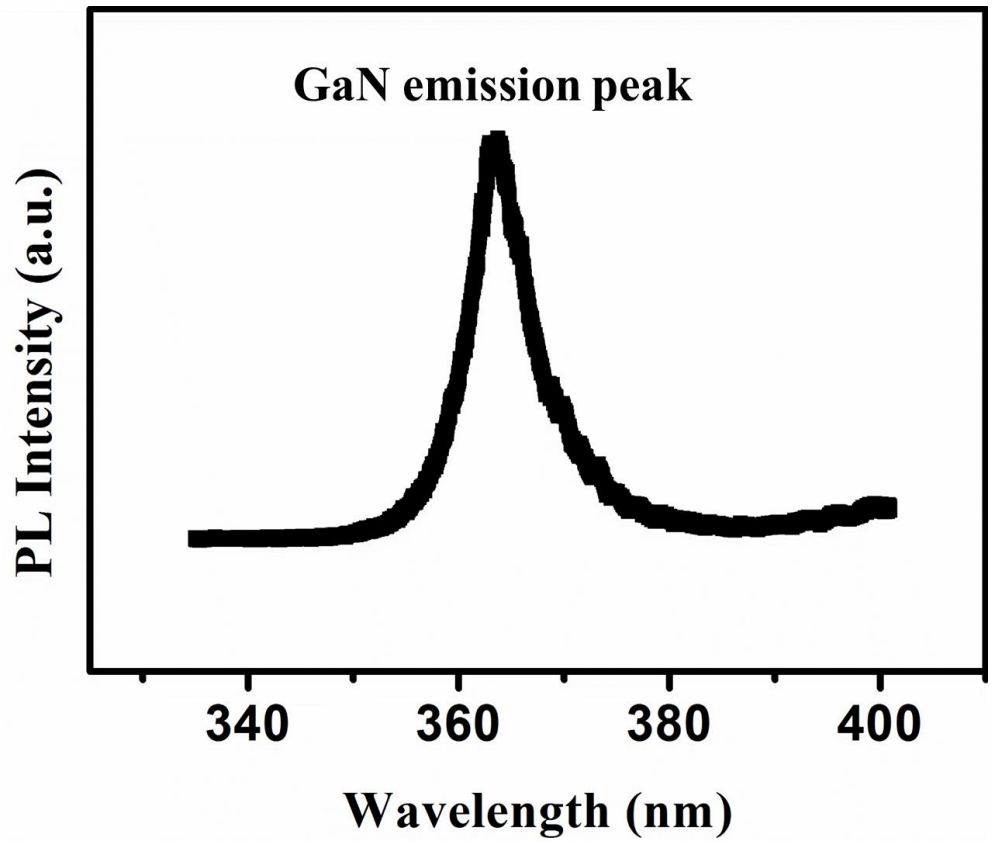

Figure 3.8: PL spectra of molecular beam epitaxially grown GaN film.

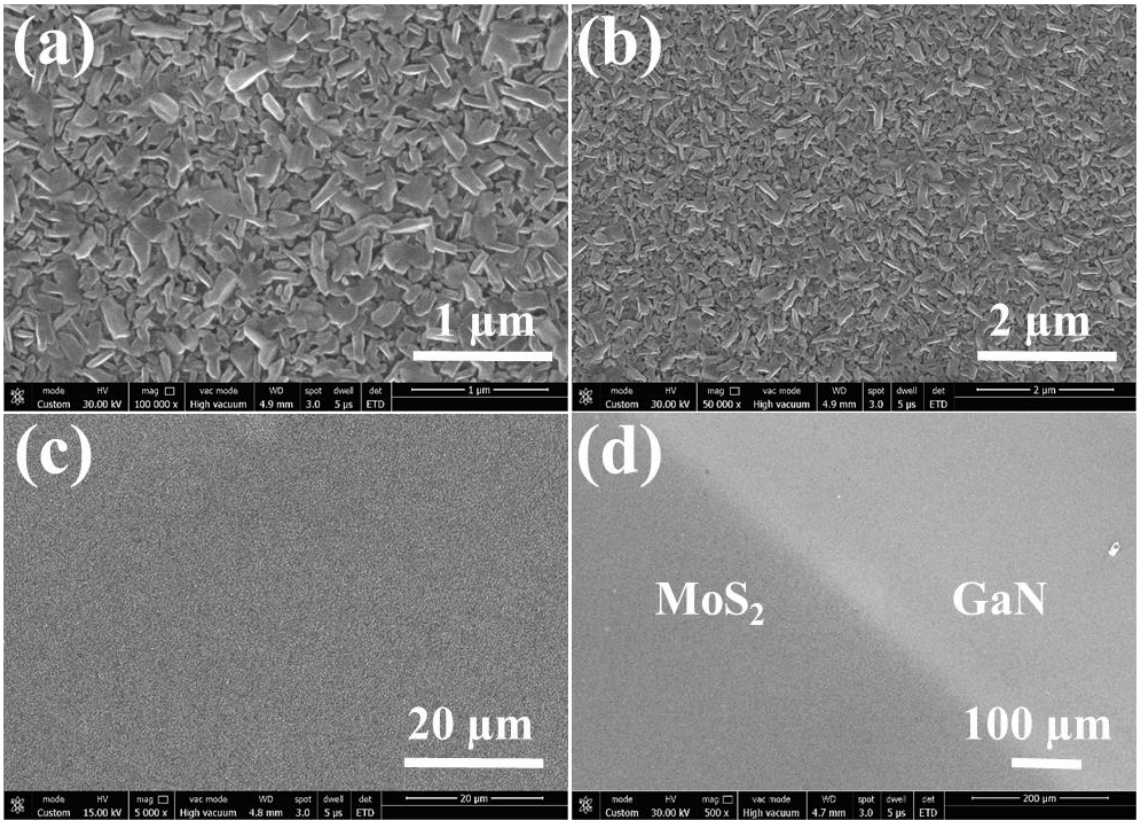

Figure 3.9: FE-SEM images of MoS_2 deposited on GaN film (a-c) at the central zone with different magnifications and (d) at the MoS_2/GaN edge.

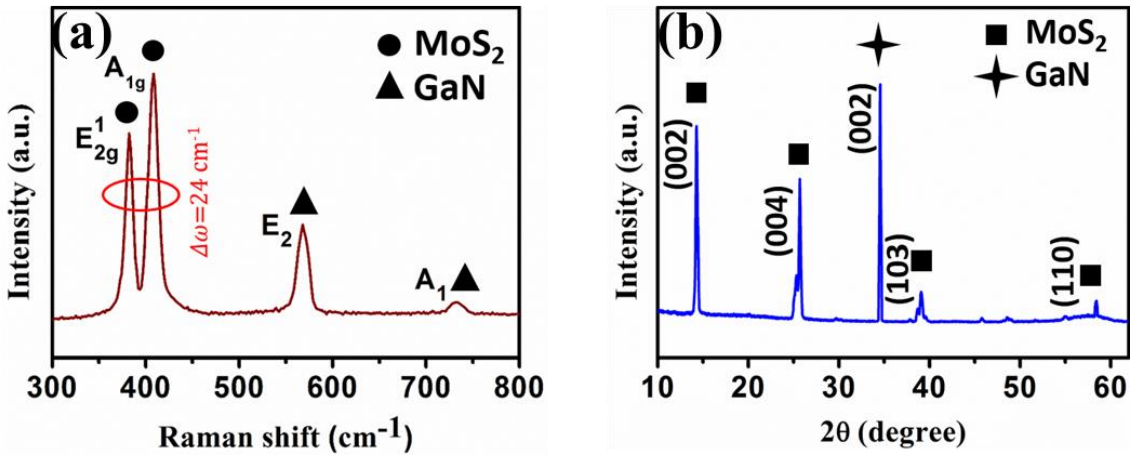

Figure 3.10: (a) Raman spectra of MoS_2/GaN interface measured by using a 514 nm laser excitation. (b) XRD patterns of MoS_2/GaN heterojunction.

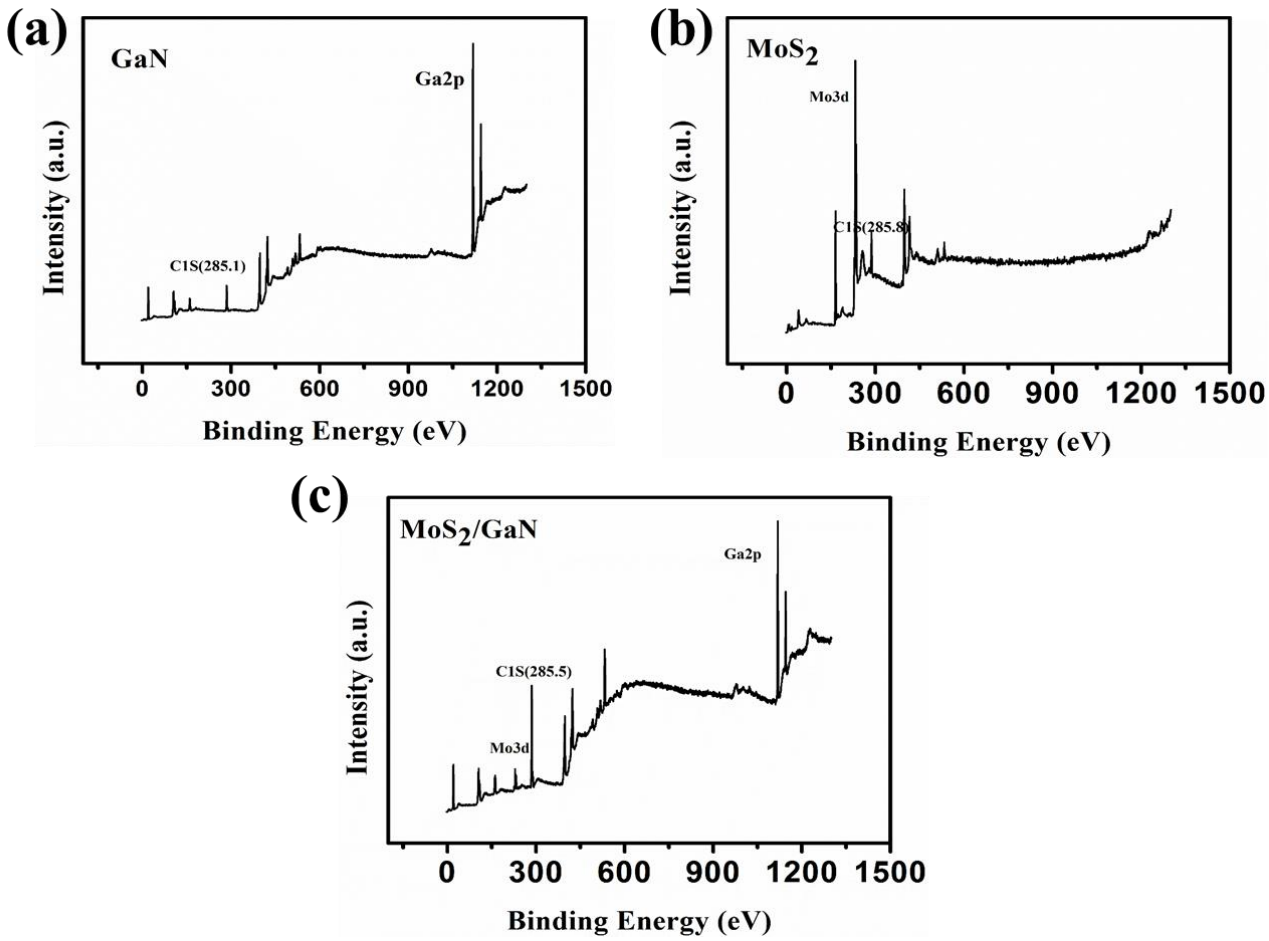

Figure 3.11: XPS survey scan of (a) GaN, (b) MoS_2, and (c) MoS_2/GaN.

3.3.2 Calculation of VBO through XPS measurement

XPS is proved to be one of the most commonly used technique for the calculation of VBO values of a conventional heterojunction. This method requires to measure the core-level energy difference between Ga and Mo constituents across the interface and the core-level positions of the MoS_2 and GaN with respect to their valence band maximum (VBM) positions. However, acquiring VBO by using this method poses two major challenges. The principal challenge is that the thickness of the deposited MoS_2 over the GaN substrate has to be thin enough to allow emission of electrons from both the constituent semiconductors at the heterojunction. This problem was resolved by sputtering a 4 nm thick Mo film on the GaN

substrate since the thickness of the deposited MoS_2 film was decided by the thickness of the sputtered Mo film. Secondly, the surface area of the deposited MoS_2 film has to be large enough in size to satisfy the minimum analysis area range of XPS measurement(Chiu et al., 2015). This challenge has been addressed by preparing a large-area and continuous MoS_2 film via the magnetron sputtering process.

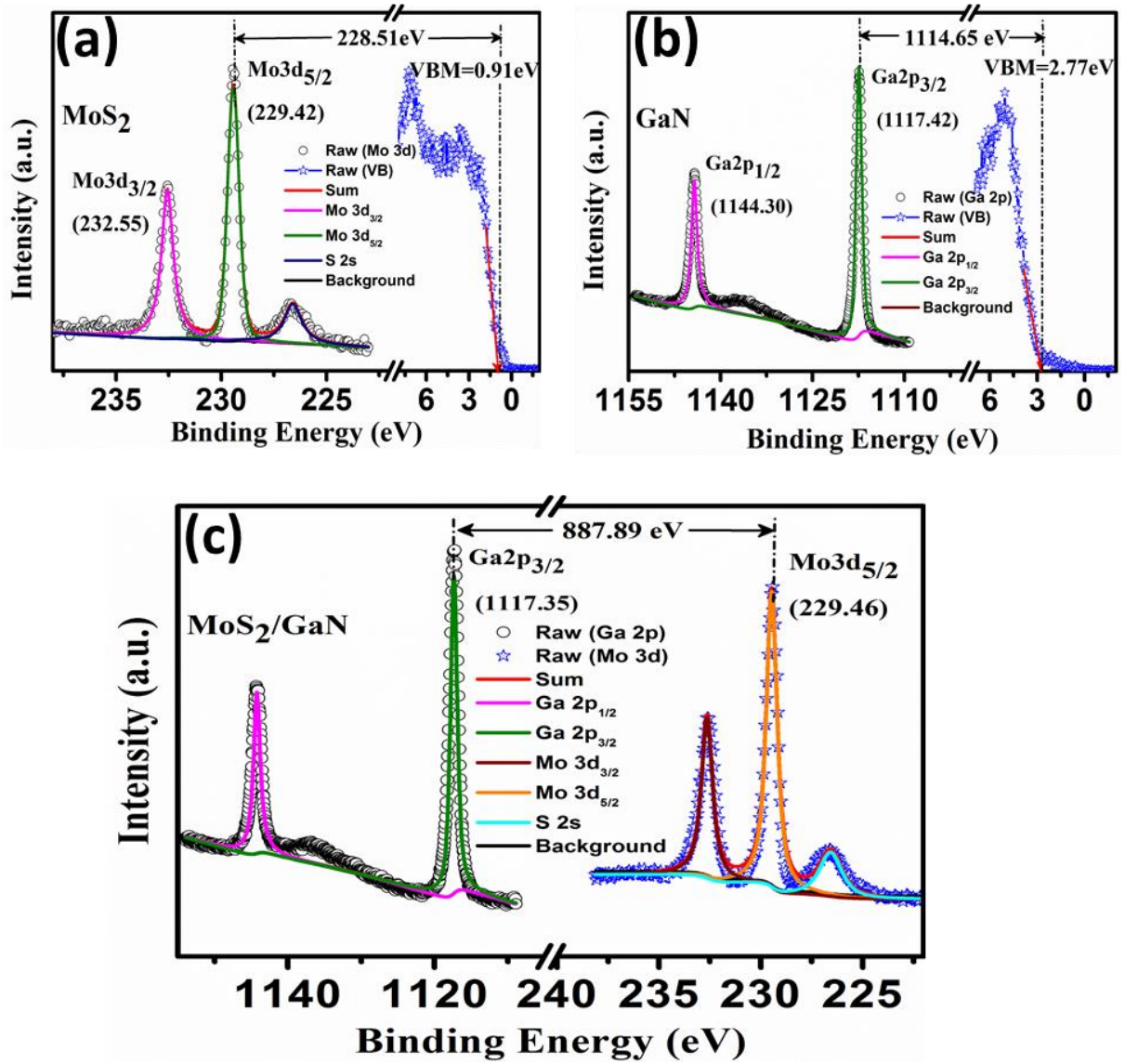

Figure 3.12: (a) Mo 3d core-level and valence band spectra obtained from MoS_2 film. (b) Ga 2p core-level and valence band spectra of molecular beam epitaxially grown GaN film. (c) Spectra of Ga 2p and Mo 3d core-level acquired on the stacked MoS_2/GaN heterojunction. Core-levels and valence band spectra are recorded from X-ray photoelectron spectroscopy (XPS) measurement.

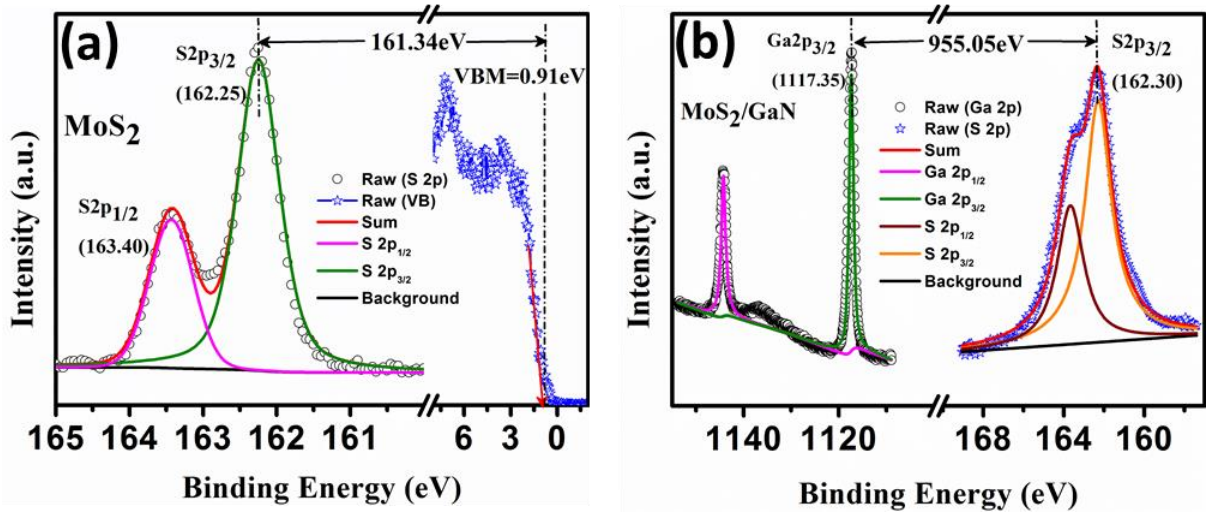

Figure 3.13: (a) S 2p core-level and valence band spectra of MoS_2 Film. (b) Ga 2p and S 2p core-level spectra obtained from stacked MoS_2/GaN heterojunction.

To calculate the value of VBO, we have taken into consideration the core-levels of Mo3d and Ga2p of individual MoS_2, individual GaN, and the MoS_2/GaN heterojunction, as shown in Figure 3.12(a-c). The respective VBM of individual MoS_2 and GaN are also shown in Figure 3.12(a and b). The VBO at the MoS_2/GaN heterojunction can be estimated by taking into account Mo3d and Ga2p core levels and using Kraut's relation, which is given as(Kraut et al., 1980):

$$\Delta E_v = \left(E^{MoS_2}_{Mo3d_{5/2}} - E^{MoS_2}_{VBM}\right) + \left(E^{GaN}_{Ga2p_{3/2}} - E^{MoS_2}_{Mo3d_{5/2}}\right) - \left(E^{GaN}_{Ga2p_{3/2}} - E^{GaN}_{VBM}\right) \qquad (3.4)$$

The first term on the right-hand side measured the energy difference between the Mo3d5/2 core-level and the VBM in MoS_2, which is estimated to be 228.51 ± 0.10 eV. The VBM values are determined by the least-square fitting of the linear leading edges of the valance band spectra(King et al., 1998). The VBM positions are estimated to be 0.91 and 2.77 eV for MoS_2 and GaN (Figure 3.12(a and b)), respectively. The subsequent term on the right-hand side of Eq. (3.4) can be estimated by taking into account the difference between $Ga2p_{3/2}$ and $Mo3d_{5/2}$, which is determined to be 887.89 ± 0.10 eV, as shown in Figure 3.12(c). The last term measured the $Ga2p_{3/2}$ core level with respect to the VBM position in GaN and estimated to be 1114.65 ± 0.10 eV. By substituting all the terms of Eq. (3.4) with their respective values, the VBO is measured to be 1.75 ± 0.17.

In addition, to reaffirm the obtained value of VBO, we have taken into consideration the valance band spectra and value of S2p and Ga2p core-levels, as shown in Figure 3.13 (a and b). The VBO from S2p and Ga2p core-levels can be estimated as:

$$\Delta E_v = \left(E^{MoS_2}_{S2p_{3/2}} - E^{MoS_2}_{VBM}\right) + \left(E^{MoS_2/GaN}_{Ga2p_{3/2}} - E^{MoS_2/GaN}_{S2p_{3/2}}\right) - \left(E^{GaN}_{Ga2p_{3/2}} - E^{GaN}_{VBM}\right) \qquad (3.5)$$

The first, second, and third term on the right-hand side of Eq. (3.5) indicate the position of $S2p_{3/2}$ core-level relative to VBM in MoS_2, the energy difference between $Ga2p_{3/2}$ and $S2p_{3/2}$ core-levels, and the position of $Ga2p_{3/2}$ core-level relative to its VBM, respectively. Therefore, the value of VBO from Eq. (3.5) is calculated to be 1.74 ± 0.17 eV, which is consistent with the VBO value acquired by using Mo3d and Ga2p core-levels.

The VBO measurement of MoS_2/GaN heterojunction also allows us to determine the value of CBO by taking cognizance of bandgap (E_g) of FL-MoS_2 and GaN, using the following expression:

$$\Delta E_c = E_g^{GaN} - \Delta E_v - E_g^{MoS_2} \quad (3.6)$$

Where $E_g^{MoS_2}$ is the bandgap of MoS_2 (1.35 eV), and E_g^{GaN} is the bandgap of GaN (3.4 eV)(Goel et al., 2018; Zhuo et al., 2018). Thus, by substituting the values of bandgaps in Eq. (3.6), CBO is estimated to be 0.30 ± 0.17 eV.

3.3.3 Calculation of CBO through UPS measurement

the acquired value of CBO can further be verified by calculating the electron affinities of the constituent semiconductors through UPS measurement. The electron affinities can be determined as follows:

$$\chi = h\nu - W - E_g \quad (3.7)$$

where hν is the photon energy of the He-I resonance line (21.22 eV), produced when light emitted from neutral atoms; W is the emission width which is calculated from low energy cut-off positions of the secondary electrons to the VBM as described in Figure 3.14 (a and b); and E_g is the bandgap of the constituent semiconductors present at the heterojunction interface. By using Eq. (3.7), the electron affinities values of 4.29 ± 0.10 and 4.01 ± 0.10 eV was acquired for MoS_2 and GaN, respectively. Our obtained values of electron affinities are in good agreement with the earlier reported literature values(Larentis et al., 2014; Li et al., 2016). Thus, we can measure the values of CBO using Anderson's affinity rule, which states that the difference between electron affinities of the constituent semiconductors gives the CBO value(Anderson, 1960). By considering the calculated values of electron affinities, CBO is estimated to be 0.28 ± 0.10 eV at the MoS_2/GaN interface.

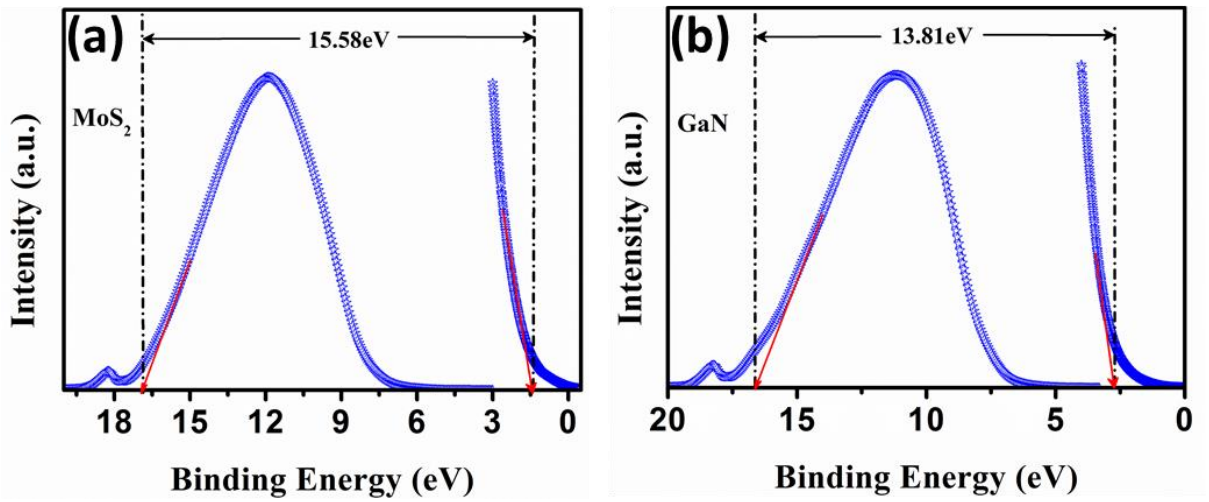

Figure 3.14: Ultraviolet photoelectron spectroscopy (UPS) spectra of (a) as-grown MoS_2 film and (b) molecular beam epitaxially grown GaN film.

The obtained value of CBO by Anderson's affinity rule is consistent with that obtained by Eq. (3.6). Therefore, the experimentally determined values of VBO and CBO through XPS and UPS measurements affirm a type-I band alignment across the MoS_2/GaN heterojunction interface, as shown in Figure 3.15.

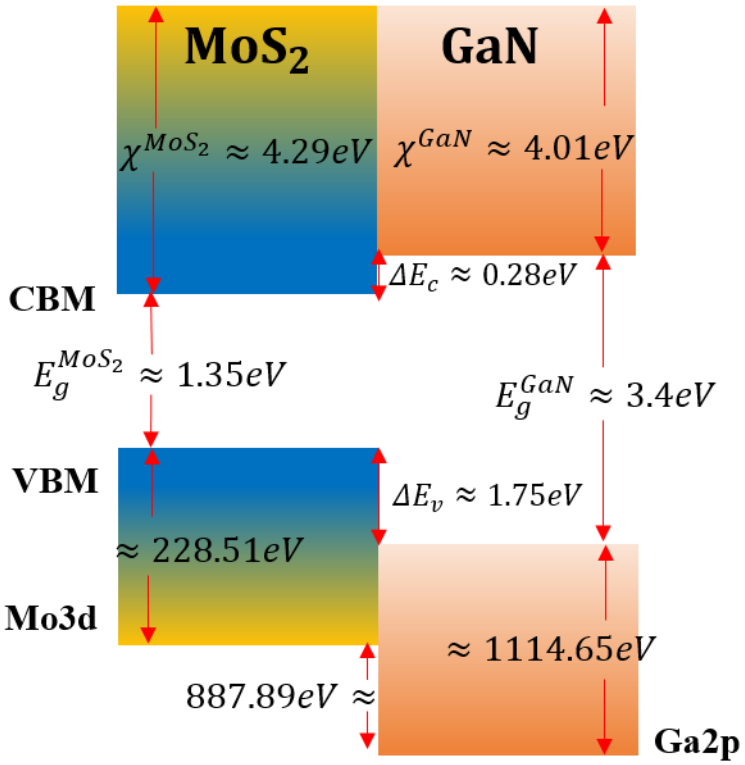

Figure 3.15: Schematic illustration depicting experimentally derived type-I band alignment at FL-MoS_2/GaN heterojunction.

3.4 COMPARISON OF INTERFACIAL ELECTRONIC MOVEMENT AT MoS_2/Si AND MoS_2/GaN HETEROINTERFACES

The shifts in the Fermi level and core levels of MoS_2 and GaN at the MoS_2/GaN heterojunction with referenced to the Fermi level and core level positions of individual MoS_2 and GaN samples can be explained with the help of electronic structure at the heterointerface. To have a better understanding, we have compared the results obtained at MoS_2/GaN heterojunction with our previously reported outcomes at MoS_2/p-Si heterojunction(Goel et al., 2018). Once the physical contact is formed between MoS_2 and p-Si, the smaller work function of MoS_2 allows the electron transfer to the underlying silicon substrate, as shown in Figure 3.16(a). Subsequently, an upward band-bending near the MoS_2 surface and downward band-bending near the Si surface will take place to align the Fermi-levels of both the constituent semiconductors. Whereas the opposite nature of the movement of interfacial electrons was observed when a thin layer of MoS_2 and lower work function GaN stacked together, as shown in Figure 3.16(b).

The Fermi level of MoS_2 starts moving toward the conduction band minimum due to charge transfer from the lower work function GaN surface. At the MoS_2/GaN heterojunction, MoS_2 is not fully depleted. Thus, a downward band-bending is expected near the MoS_2 surface. Since the XPS reflect the core level binding energies relative to the Fermi level, the shifting of the peak positions of $Mo3d_{5/2}$ and $Ga3p_{3/2}$ are consistent with the interfacial electron transfer from GaN to the stacked MoS_2 film. Lin et al. have also illustrated a band bending at the interface and a shifting in the core energy levels of the constituent semiconductors when MoS_2 and a thin layer of lower work function Cs_2CO_3 makes a heterostructure(Lin et al., 2014).

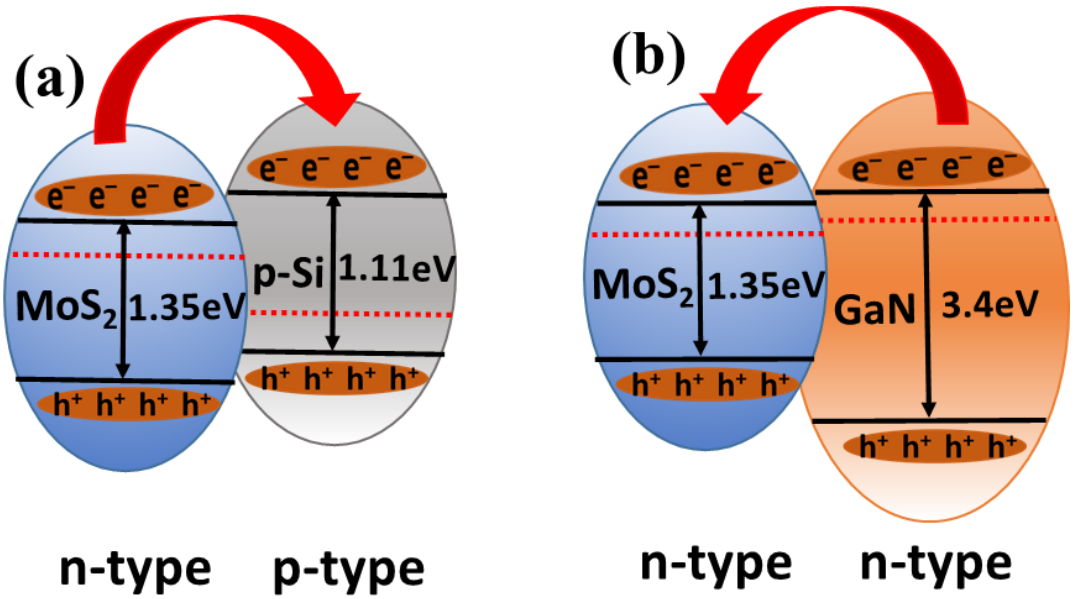

Figure 3.16: Comparison of interfacial electronic movement at (a) MoS_2/p-Si and (b) MoS_2/GaN heterojunctions.

3.5 CHAPTER SUMMARY

In summary, we have successfully studied the band alignment at the MoS_2/Si and MoS_2/GaN heterojunctions using XPS and UPS measurements by determining the CBO and VBO values at the interfaces. We determined a type-II and type-I band alignments at the MoS_2/Si and MoS_2/GaN heterojunction, respectively, which will be very conducive to fabricating light-emitting diodes and lasers by spatially confining the charge carriers. The determination of band offset parameters paves the way for the integration of TMDs with other dimensional semiconductors for futuristic high-performance optical devices.

…

4

Enhanced Carrier Density in a MoS_2/Si Heterojunction-based Photodetector by Inverse Auger Process

4.1 INTRODUCTION

In recent years, TMDs have established themselves as potential constituents for optoelectronics applications because of their mechanical flexibility and transparency (Baugher et al., 2014; Wang et al., 2012; Zhang et al., 2014). As one of the most influential members of the TMDs family, MoS_2 proves to be of significant importance in the context of optical devices due to its tunable bandgap, high carrier mobility, significant absorption coefficient, the favorable rate of electron-hole (e-h) pair generation, and immense current carrying capacity (Bernardi et al., 2013; Chu et al., 2015; Kim et al., 2012; Liu et al., 2013). In addition, the bandgap tuning in MoS_2 either by changing the number of layers or by electric field facilitates the detection of light at various wavelengths (Lu et al., 2014). A large number of optoelectronic applications based on MoS_2 have already been addressed, for instance, photovoltaic devices, light-emitting diodes, optical modulators, and plasmonic devices (Li et al., 2017; Pospischil and Mueller, 2016; Zhang et al., 2015). Among these applications, the development of hybrid photodetectors based on different vdW heterostructures gains much attention owing to their high performance, including an excellent photo-responsivity and high external quantum efficiency. MoS_2 heterojunction-based photodetectors showed a maximum external photo-responsivity in the range of 8.8×10^2–1.2×10^7 A/W (Lopez-Sanchez et al., 2013; Zhang et al., 2014).

2D layered materials can be used to form a vdW heterojunction with materials of different dimensionalities, such as 0D/2D, 1D/2D, and 3D/2D (Jariwala et al., 2016). The performance of these 2D materials can be significantly enhanced by employing a hybrid heterojunction with other nanomaterials. These hybrid structures prove to be an essential component for commercial applications in optoelectronics and light-harvesting technologies because of their tunable properties and the absence of dangling bonds at the interface (Allain et al., 2015). MoS_2-based hetero-junction has received considerable attention because of its unique electrical and optical properties (Jariwala et al., 2016; Wang et al., 2016). A contact between a few-layer MoS_2 (FL- MoS_2) and n-Si can create a barrier at the interface. The electronic cloud of Mo is to be perturbed by the n-doped silicon Fermi level, resulting in the creation of an energy barrier between them. The formation of an energy barrier between n-Si and n-type ZnO has already been reported in the earlier reports (Ranwa et al., 2014; Ranwa et al., 2014). The photo-induced charge carriers have to overcome this barrier in order to contribute to the photocurrent. As the bandgaps of Si and FL-MoS_2 are 1.1 eV and 1.3 eV, respectively, visible light can excite electrons from both semiconductors. Thus, the photo-induced electrons from MoS_2 and Si can contribute to the total photocurrent. However, as the wavelength varies from visible to infrared region, the photocurrent is reduced due to the insufficient photo energy to cross the barrier. Moreover, despite their great potential, FL-MoS_2 has not been extensively studied, and most of the research is focused only on monolayer MoS_2. In this study, we choose FL-MoS_2 because of its higher absorption rate of incident photons, large current carrying capacity, a higher density of states, and favorable mobility.

The principle of photodetectors is based on the generation and recombination of e-h pairs at the junction. Hence, it is essential to understand the charge transport mechanism in photodetectors in order to investigate the optical behavior of the device. Although there are